Published in final edited form as:
J Mol Biol. 2012 August 10; 421(2-3): 242–255. doi:10.1016/j.jmb.2011.12.016.

Amyloid fibril formation by the glaucoma-associated olfactomedin domain of myocilin

Susan D. Orwig[1], **Christopher W. Perry**[1], **Laura Y. Kim**[2], **Katherine C. Turnage**[1], **Rong Zhang**[3], **Douglas Vollrath**[3], **Ingeborg Schmidt-Krey**[1,2], and **Raquel L. Lieberman**[1,*]

[1]School of Chemistry & Biochemistry, Stanford University School of Medicine

[2]School of Biology, Georgia Institute of Technology, Stanford University School of Medicine

[3]Department of Genetics, Stanford University School of Medicine, Stanford University School of Medicine

Abstract

Myocilin is a protein found in the extracellular matrix of the trabecular meshwork (TM) tissue, the anatomical region of the eye involved in regulating intraocular pressure. Wild-type (WT) myocilin has been associated with steroid-induced glaucoma, and variants of myocilin have been linked to early-onset, inherited glaucoma. Elevated levels and aggregation of myocilin hasten increased intraocular pressure and glaucoma-characteristic vision loss due to irreversible damage to the optic nerve. In spite of the reports of intracellular accumulation of mutant and WT myocilin in vitro, cell culture and model organisms, these aggregates have not been structurally characterized. In this work, we provide biophysical evidence for the hallmarks of amyloid fibrils in aggregated forms of WT and mutant myocilin, localized to the C-terminal olfactomedin (OLF) domain. These fibrils are grown under a variety of conditions in a nucleation dependent, self-propagating manner. Protofibrillar oligomers and mature amyloid fibrils are observed in vitro. Full-length mutant myocilin expressed in mammalian cells forms intracellular amyloid-containing aggregates as well. Taken together, this work provides new insights into and raises new questions about the molecular properties of the highly conserved OLF domain, and suggests a novel protein-based hypothesis for glaucoma pathogenesis for further testing in a clinical setting.

Keywords

myocilin glaucoma; olfactomedin; amyloid; aggregation; protein misfolding

Introduction

The molecular origins of glaucoma, the prevalent neurodegenerative ocular disorder characterized by a loss of visual field, are poorly understood[1]. Typically, the hallmark retinal degeneration within the optic nerve is preceded by an increase in intraocular pressure (IOP)[2], which is caused by changes in the circulation of aqueous humor in the anterior region of the ageing eye, particularly in the drainage of fluid through the trabecular

*Corresponding author (R. L. L.): raquel.lieberman@chemistry.gatech.edu, phone: (404) 385-3663, fax: (404) 894-2295.

meshwork (TM)[3]. The optic nerve damage cannot be ameliorated, but current treatments that reduce IOP slow glaucoma onset and progression[4]. Thus, an understanding of the complex mechanisms that change the overall resistance could lead to better treatments for this heterogeneous disorder.

Emerging evidence supports the hypothesis that the autosomal dominant, early-onset form of glaucoma caused by genetic defects in myocilin[5; 6], a ~57 kDa protein found in the TM and other locations[1; 5], constitutes a proteinopathy. First, amino-acid changing mutations in the gene encoding for myocilin predispose the myocilin protein to aggregation into a detergent insoluble species[7]. Several studies note intracellular sequestration of mutant myocilin[8; 9; 10; 11]. Some studies further report an endoplasmic reticulum (ER) stress response[12; 13], including explicit colocalization of large juxtanuclear myocilin aggregates with known ER chaperones[9; 14] leading to apoptosis and cell death[9; 13; 14]. The majority of myocilin variants examined, located in the ~30 kDa myocilin C-terminal olfactomedin domain (myoc-OLF)[5], thermally destabilize the domain but in vitro retain secondary structure similar to wild-type (WT); age of diagnosis follows the extent of destabilization of myoc-OLF[15]. At physiological temperatures, a less stable myocilin variant may accumulate a partially unfolded population, which should be cleared by ER associated degradation (ERAD)[16]. It appears that for myocilin variants, clearance mechanisms of the aggregation-prone unfolded protein are insufficient to prevent downstream cellular effects. Second, consistent with a gain of toxic function, diminished secretion of WT myocilin is observed when WT and mutant myocilin are co-expressed[17], demonstrating that mutant myocilin can recruit WT myocilin to generate a pathogenic response in heterozygotes. Conversely, neither individuals harboring a rare N-terminal truncation mutation[18] in myocilin, nor myocilin knock-out mice[19], exhibit glaucoma symptoms. Finally, rescue of myocilin stability and cellular trafficking by chemical chaperones has been demonstrated in vitro[20], in cells[21; 22], and very recently, in mice[23], lending further credibility to hypothesis that myocilin glaucoma is a protein conformational disorder.

Even though myocilin is not a susceptibility gene for sporadic forms of glaucoma[24], WT myocilin is associated with aggregation and glaucoma symptoms when present at high levels[25]. Prior to genetic linkage studies, and in an effort to understand steroid-induced glaucoma, myocilin was identified as a dexamethasone-induced protein in cultured human TM cells[26]. In addition, when overexpressed in the eyes of transgenic flies, myocilin aggregates in the ER, and the unfolded protein response is induced[27]. These studies raise the possibility that WT myocilin aggregation could be involved in age-onset glaucoma as well, a process that would be accelerated in the presence of mutations, or other destabilizing conditions such as oxidative and mechanical stress that are well-documented in open angle glaucoma[28].

In spite of the observations of mutant and WT myocilin aggregates in vitro and cell culture, they have not been structurally characterized. Here we demonstrate that aggregated forms of WT and mutant myoc-OLF exhibit hallmarks of amyloid fibrils. These fibrils are generated under a variety of conditions in a nucleation dependent, self-propagating manner. Both protofibrils and mature amyloid fibrils are observed in vitro. Mutant full-length myocilin expressed in mammalian cells forms intracellular aggregates containing amyloid fibrils as well, linking our conclusions in vitro to the body of work that proposes the pathogenic nature of myocilin aggregation for glaucoma. Taken together, this work provides new insights into the biophysical properties of myocilin and suggests a novel molecular-based hypothesis for glaucoma pathogenesis.

Results

Initial identification of an amyloid-containing species from maltose binding protein (MBP)-OLF fusions purified from E. coli

From our original preparative-yield expression system, we noted that after purification by amylose affinity column chromatography, the MBP-OLF fusion protein is fractionated by Superdex-75 size exclusion chromatography (SEC) into two well-separated species, one in the void volume corresponding to a large MBP-OLF species, and the expected MBP-OLF monomer ([20] and Figure 1a). Reducing sodium dodecyl sulfate-polyacrylamide gel electrophoresis (SDS-PAGE) confirmed that both species in the SEC chromatograph were composed exclusively of MBP-OLF[20]. The intensity of the void-volume species compared to that of the monomer was not sensitive to length of incubation time at 4 °C, freeze-thaw, concentration loaded on the column, nor did the species interconvert[20]. These observations indicated that the observed void-volume species is most likely formed prior to cell lysis and is not influenced by sample handling. When further subjected to fractionation on an SEC column with a much larger pore size, a distribution of high molecular weight MBP-OLF species is observed (Supplemental Figure S1), indicating that a large, possibly non-globular, and heterogeneous species is present in solution, distinct from the MBP-OLF monomer. A similar species eluting in the void-volume of the SEC chromatograph has further been observed for all ~30 variants of myoc-OLF studied in our lab, with varying intensity compared to monomer ([15] and see Figure 1a for examples of MBP-OLF(Y437H) and MBP-OLF(P370L) corresponding to variants associated with severe cases of glaucoma[29; 30]). Finally, the ratio of the void-volume and monomeric MBP-OLF species is consistent among purification attempts. Taken together, it appears that MBP-OLF isolated from *E. coli* is already in either the monomeric or an apparent misfolded form.

Due to the presence of this high molecular weight MBP-OLF species purified in two steps from *E. coli*, combined with the high β-sheet content for the myoc-OLF domain observed by circular dichroism (CD)[20; 31] and its predicted amyloid propensity by ZipperDB[32] (Supplemental Figure S2), we tested the hypothesis that the void-volume SEC fraction constituted amyloid. First, an increase of thioflavin T (ThT) fluorescence, which detects mature fibrils but not precursor protofibrils, monomers or amorphous aggregates[33], is observed for the MBP-OLF void-volume species over the constituent monomer (Figure 1b). Similarly, void-volume species of disease-causing MBP-OLF variants studied in our lab[15; 20] exhibit high levels of ThT fluorescence (see for two examples, MBP-OLF(Y437H) and MBP-OLF(P370L), Figure 1b). Second, treatment of the MBP-OLF void-volume species with proteinase K (PK), a protease highly active against globular or disordered proteins but not against densely packed cross-β regions[34; 35], followed by purification by SEC, reveals again a ThT positive void-volume elution peak (Figure 1a,b) composed of smaller protein segments, detected by tricine gel electrophoresis as small as ~ 3 kDa (Supplemental Figure S3). Third, transmission electron microscopy (EM) images of negatively-stained MBP-OLF void-volume samples, disease-causing variants MBP-OLF(Y437H) and MBP-OLF(P370L), and PK-treated material, reveals discs and toroids, as well as unbranched curvilinear strings of different lengths, possessing a width of ~8-11 nm similar to the dimensions of amyloid fibrils of ~10 nm[36] (Figure 1c), and morphologies similar to those observed for amyloid-β peptide (Aβ)[37; 38] and α-synuclein[39]. Consistent with this observation, we positively identified prefibrillar oligomers (Figure 1d), the pathogenic species proposed for Alzheimer[37] and Parkinson disease[39], using the sequence-independent A11 antibody that recognizes soluble oligomers and not soluble monomers, low molecular weight oligomers, or fibrils[40]. Finally, control experiments conducted to clarify that the aggregated species was a result of OLF and not MBP (not shown) are consistent with the extensive literature touting the favorable solubility profile of MBP as a fusion protein[41], the reversibility of its unfolding[42], and the ability of MBP to form of amorphous,

resoluble, non-amyloid precipitate[43]. We also note that as part of the protein purification procedure, the cytosolic MBP-OLF is stringently stripped of all insoluble material by ultracentrifugation, such that only soluble material is subjected to affinity chromatography and SEC, thus eliminating the possibility that the aggregates isolated were contaminated with amyloid-containing inclusion bodies[44].

Conditions that promote spontaneous, de novo, fibrillization of myoc-OLF in vitro

We next examined whether the cleaved, monomeric myoc-OLF alone could be converted to a fibrillar form (Figure 2). Fibril formation of myoc-OLF in mild buffer takes multiple days with gentle rocking at 37 °C ($t_{1/2}$ ~ 48 h, Figure 2a), exhibiting both the expected nucleation and extension phase[45; 46]. No fibrils are formed when myoc-OLF is incubated at 4 °C for the same time frame (Table 1) or for over a month[20]. Incubation in a circulating water bath at 37 °C, i.e. without any agitation, over a longer period of 2 weeks, does not result in an increase in ThT fluorescence consistent with fibril assembly. For myoc-OLF incubated with gentle rocking at 37 °C for 95 hr, EM images reveal typical unbranched, twisted ropes amyloid morphology (Figure 2b), consistent with the depletion of monomeric myoc-OLF, plateau of the high ThT fluorescence signal (Figure 2a), lack of protofibrillar oligomers by A11 antibody detection (not shown). The myoc-OLF(Y437H) disease-causing variant forms fibrils more readily than WT. Fibril formation proceeds without agitation in a 37 °C circulating water without a lag phase (Figure 2f, closed circles). It has proved challenging to isolate preparative quantities of myoc-OLF(Y437H) devoid of nuclei and observe the expected lag phase for fibril formation.

The nucleation process requires the self-assembly of pro-amyloid monomers, and therefore is the rate-limiting step, but fibril formation can be accelerated by exposing the protein to slightly destabilizing conditions. For example, anionic detergents such as SDS below the critical micellar concentration (0.8 mM) accelerate the kinetics of amyloid fibril formation, as seen for β_2-microglobulin[47] and α-synuclein[48; 49]. Similarly, for myoc-OLF, SDS stimulates fibril formation (Table 1) at an optimum of 0.5 mM. At concentrations above 1.0 mM, fibrillization was significantly reduced and only amorphous aggregates were observed by EM (Supplemental Figure S4). When monomeric myoc-OLF is incubated in a water bath at 30 °C in a buffer containing 0.5 mM SDS, no lag phase is observed and a plateau in ThT fluorescence is reached after 30 hrs (Figure 2d, black curve), compared to ~ 70 hr required without SDS at 37 °C (Figure 2a).

Kinetics were further investigated using preformed myoc-OLF fibrils generated, as described above, by overnight incubation of myoc-OLF with 0.5 mM SDS. These fibrils exhibited elevated ThT fluorescence and a CD spectrum with a minimum near 220 nm (Figure 2c) reported for other amyloids[38; 50]. Fibrils were fragmented into seeds by sonication and added at a 1:1 or 2:1 molar ratio to purified monomeric myoc-OLF in buffer containing 0.5 mM SDS, and incubated at 30 °C. As expected, the rates of fibril formation were accelerated ($t_{1/2}$= ~3 hrs with 1:1 seeds:monomer and $t_{1/2}$= ~1.5 hrs for 2:1 ratio, Figure 2e) compared to the rate of fibril formation without seeds (Figure 2d, black curve). The self-seeding propensity of myoc-OLF was further evaluated by conducting multiple rounds wherein the fibrillized material from a previous round was used to seed the next[51]. Each subsequent round (Figure 2d, red and blue curves) exhibited a faster rate until the third, indicating maturation of the fibrils had been achieved. Finally, seeds of myoc-OLF can readily template the fibril formation of myoc-OLF(Y437H) (Figure 2f, open circles), at a rate faster than without additional seeds. This result suggests that the underlying amino acids responsible for fibrils are present in both WT and the disease-causing variant.

We attempted to mimic *in vitro* the oxidative stress expected during the aging eye process[52; 53] that may promote fibrillization by treating myoc-OLF with varying

concentrations of hydrogen peroxide. The addition of 1.5% hydrogen peroxide led to a high level of ThT fluorescence after 24 hr compared to when no peroxide was present for 95 hr (Table 1). Fibrils of peroxide-treated myoc-OLF were also apparent by EM (Figure 2g). Like with SDS, higher levels of peroxide beyond an upper limit led to decreased ThT fluorescence and amorphous aggregates by EM (data not shown).

Identification of full-length myocilin amyloids from mammalian cell culture

We found evidence for amyloid fibrils derived from mammalian cell culture expressing full-length myocilin by ThT staining of intact cells[54] and by using a boiled-gel electrophoretic mobility experiment described for yeast prions[55]. The latter boiled-gel assay relies on the fact that low concentrations of SDS (1%) are insufficient to disaggregate amyloids, causing them to migrate poorly, if at all, through the resolving SDS-PAGE gel; applying steam to the jammed amyloid fibrils results in their disaggregation and migration into the gel upon a second electrophoresis step. Poor and heterogeneous electrophoretic migration is also known for Aβ[56], and has been seen for Triton X-100 (TX)-soluble and TX-insoluble aggregates of several other glaucoma-causing myocilin variants (D380A, E323K, Y437H, G364V, and K423E) expressed in mammalian cells where higher SDS concentrations in the loading buffer were used[9].

For the gel mobility experiment, equivalent amounts of total protein from TX-soluble and TX-insoluble forms of myocilin[7] isolated from CHO cells were applied to lanes of an SDS-PAGE gel and after electrophoresis, analyzed by immunoblot via a C-terminal S-tag. It is apparent that the TX-insoluble sample of myocilin(P370L) variant contains more myocilin than the other lanes, and some material does not appear to have entered the resolving gel at all (Figure 3a, left). This trapped species was observed to a lesser extent in the TX-soluble sample of myocilin(P370L) and TX-insoluble WT myocilin samples but not in vector control nor in TX-soluble WT samples (Figure 3a, left). After disaggregation by steam, the aggregated samples entered the resolving gel (Figure 3a, right). An analogous migration pattern was obtained using *in vitro* MBP-OLF aggregates (Supplemental Figure S5).

To explicitly test for myocilin amyloid in cell culture, CHO cells expressing either WT or the P370L myocilin variant were stained with ThT and observed under a fluorescent microscope[54]. There was minimal ThT fluorescence in the WT sample (Figure 3b, top panels), signifying low levels of amyloid fibrils formed as a result of myocilin overexpression. By contrast, CHO cells transfected with P370L-mutant myocilin exhibited strong ThT fluorescence (Figure 3b, bottom panels), consistent with results obtained in vitro (Figure 1). There was no discernible extracellular staining for either sample.

Localization of the amyloidogenic protein sequence within OLF

To date, our attempts to identify the amino acid sequence(s) responsible for myoc-OLF fibril formation by N-terminal sequencing or mass spectrometry have not yielded unambiguous results (data not shown). As an alternative approach, we attempted to localize the amyloidogenic core(s) by systematically assembling the myoc-OLF domain in ~20 residue segments by C-terminal fusion to MBP (Figure 4, Supplemental Figure S6). After amylose affinity purification of these MBP constructs isolated from the *E. coli* cytosol, fractionation by SEC was employed to identify void-volume species analogous to MBP-OLF isolated from *E. coli* (Figure 1a). Surprisingly, the construct containing the first 17 residues (MBP-$OLF_{228-244}$) (Figure 4a,b), as well as all larger constructs tested, yielded void-volume SEC species with high ThT fluorescence (Figure 4c,d, Supplemental Figure S6a,b). As observed by SEC, fibril formation was abrogated when a stop codon was introduced in the middle of MBP-$OLF_{228-244}$, at Tyr 235 (Figure 4a, blue), to create MBP-$OLF_{228-234}$ (Figure 4b-d, red). Incubation of either MBP or MBP-$OLF_{228-234}$ under conditions for facile OLF

fibrillization (95 hrs at 37 °C in the presence of 0.5 mM SDS) did not lead to an increase ThT fluorescence (Figure 4e), indicating that neither accumulated appreciable levels of mature fibrils, especially when compared to myoc-OLF and MBP-OLF (Figure 1a) evaluated under identical assay conditions. The ability of the N-terminal region of myoc-OLF to form a ThT-positive aggregate was unexpected because this region is only weakly predicted to form amyloids *in silico* (Supplemental Figure S2).

Additional fibril forming segments beyond the N-terminal 17 amino acids were identified with two more constructs (Figure 4c,d). First, a truncated version lacking the first 17 residues (MBP-$OLF_{245-504}$) (Figure 4a,b, green) was generated, resulting in a ThT-fluorescent void-volume species by SEC. Second, the N-terminally truncated construct was further shortened at its C-terminus to mimic the structural core-OLF domain[31], generating MBP-$OLF_{245-455}$ (Figure 4b, orange). Again, a ThT-fluorescent void-volume species was observed by SEC (Figure 4c,d). These results point to the strong possibility that at least one more amyloidogenic sequence resides within the structural core of the myoc-OLF domain, specifically between residues 245 and 455, but does not exclude the possibility that an amyloidogenic stretch is also present in the removed C-terminal residues (456-504). Future work will be focused on elucidating which of the numerous predicted and possibly cryptic amyloidogenic stretches exist for myoc-OLF.

Discussion

Amyloid formation, in which a seemingly innocuous protein is converted to a fibrillar form, is recognized as a major contributor to numerous human diseases[57], including those of the eye (reviewed in[58]), such as the in the lens (cataract), and the in retina (age-related macular degeneration). The deposition of disease-relevant amyloids from non-ocular diseases, such as Alzheimer disease (amyloid precursor protein[59], Aβ[60] and tau[61]) and Creutzfeldt-Jacob disease (scrapie protein[62]) within a variety of ocular tissues, has been observed as well. To date, amyloid contributions to glaucoma have been restricted to Aβ, which have been specifically implicated in retinal ganglion cell death[60]. The addition of myocilin expands the context in which to explore amyloid deposits as a molecular basis of both inherited and sporadic glaucoma, as discussed below. Future treatments could include drugs that prevent or stop myocilin amyloid formation, or degrade existing fibrils.

Indeed, recombinant WT myoc-OLF is a stable, monomeric globular domain with high β-sheet content that can be converted to a fibrillar morphology under mild conditions. While there is no definitive test for amyloid, an assortment of MBP-OLF and myoc-OLF variants exhibit several of the tell-tale signatures of amyloid. These features include tinctorial affinity for the ThT dye, resistance to proteolysis by the promiscuous PK, as well as curvilinear, toroidal, and twisted roped-shape aggregates seen by EM, recognition by the oligomer-specific A11 antibody, and limited electrophoretic mobility in SDS-PAGE. Monomeric, WT myoc-OLF can spontaneously form fibrils that appear as intertwined ropes within a few days, in the nucleation-specific manner expected of an amyloid when incubated under physiological conditions with only gentle rocking. Destabilizing conditions such as low concentrations of SDS form ThT-positive fibrils that exhibit a familiar CD signature, and these seeds accelerate myoc-OLF fibril formation with rates altered by their concentration. The myoc-OLF(Y437H) variant, which is significantly less stable (Tm ~43 °C) than WT (Tm ~54 °C)[15], forms fibrils more readily, and agitation is not required. Further, cross-seeding reactivity with WT is suggestive of a common amyloidogenic peptidic core that can recruit new monomer, possibly providing an explanation for the dominant glaucoma phenotype exhibited by individuals heterozygous for myocilin mutations.

In agreement with the findings from myoc-OLF expressed in *E. coli*, ThT-positive amyloid fibrils accumulate intracellularly when full-length myocilin harboring the P370L lesion, is expressed in CHO cells. Our observations in cell culture link our conclusions in vitro to the body of studies that point to the disease-relevance of myocilin aggregation. Notably, the full-length myocilin protein, approximately twice the size of the OLF domain alone, harbors an N-terminal region with a coiled-coil for dimerization. Future directions will include validating fibril formation by myocilin in vivo, verifying myoc-OLF as the site of fibril formation for full-length myocilin, as well as elucidating whether kinetics of amyloid formation are altered by the presence of the N-terminal region and/or by having OLF domains in close proximity.

The TM provides a microenvironment primed to facilitate WT myocilin fibril formation. Over time, the filter-like region of the inner TM loses efficiency at clearing debris, rendering the juxtacanalicular region of the TM, the site of aqueous humor outflow, partially obstructed[63]. The morphological changes to the TM in the aging eye, which are due in part to loss of TM cells (see below), are thought to underlie the increase in IOP leading to glaucoma. Interestingly, myocilin is one of the more highly expressed matricellular proteins[64] present in the juxtacanalicular tissue of the TM[65], where it interacts with extracellular matrix proteins and modulates cell-matrix interactions[66; 67]. Immunohistochemical analysis of TM tissue from patients reveals fine fibrils in both steroid- and open angle glaucoma that have been attributed in part to collagens[68], a known facilitator of fibril formation[69]. Similarly, among the many cofactors known to enhance or influence amyloid fibril formation[70], glycosaminoglycans in the extracellular millieu can provide a scaffold for myocilin fibril formation[71; 72; 73]. It is not known to what extent TM changes after loss of TM cells are due to dysregulation of free radical species, loss of ability to remodel after mechanical stress, toxicity of stress response elements when present on a chronic basis, or protein modification[63], but we have shown that myoc-OLF domain readily forms fibrils with mild destabilization by SDS or peroxide. The contribution of fibrils of WT myocilin, both within the juxtacanalicular and other regions of the TM, to the detrimental changes in TM morphology with aging will be an interesting line of inquiry in model and patient-derived systems.

TM cell loss that contributes to morphological changes in the TM extracellular matrix may be due to challenges to function and maintenance of homeostasis upon the accumulation of amyloid-forming myocilin intracellularly. This condition is expected to be significantly worse for TM cells expressing mutant myocilin congenitally, leading to deleterious effects much sooner. Phagocytosis, an important debris-removing function of these cells that keeps the juxtacanalicular region clear[3], is one key function likely weakened as TM cells unsuccessfully cope with removing intracellular aggregates of myocilin. Protein synthesis occurring as part of proper TM turnover is another process likely damaged. Impaired degradation[74] of myocilin aggregates presumably leads to aberrant accumulation in other relevant cellular compartments[9; 13; 14; 75; 76; 77; 78], affecting protein folding and other cellular processes more generally. Under these conditions, even degradation by autophagy[79], which, in the case of mutant myocilin may be assisted by peroxisomes[8], likely cannot compensate sufficiently for ERAD inhibition, leading to apoptosis[9; 13; 14]. Once TM cells die, it is straightforward to foresee that cellular debris would be detrimental to TM function and proper outflow, leading to IOP elevation. However, the presence of myocilin amyloid fibrils, whether mutant or WT, may compound the insult by providing a template for any natively-folded, secreted myocilin to form new fibrils. To assess the contribution of amyloid fibril formation to TM loss, localizing the intracellular fibrils and elucidating effects on cellular machinery, as well as discriminating fibril formation among different cell types, will be required, followed by identifying the toxic species. For example, although to date TM cells seem to be the primary cell type affected by aberrant behavior myocilin, an intriguing

possibility is that myocilin amyloid deposition in other glaucoma-relevant regions of the eye, such as the optic nerve, could have direct toxic effects.

Aside from its association with glaucoma, the normal biological function of myocilin and OLF domain, as well as its structure, and folding or unfolding pathway, remain rather enigmatic yet highly intriguing, particularly now in light of its proclivity to convert to an amyloid form. The importance of elucidating these features for the OLF domain is underscored by its conservation among higher eukaryotes. OLF domains are prevalent in neural tissue[80], are involved in chemoreception[81], cell-cell[82] cell-matrix interaction[83], and are implied in gastrointestinal cancers[84] among other roles; yet, many details, such as binding partners, are missing[80]. From what is known about OLF structure based on in silico prediction[85], the OLF domain harbors a poorly-predicted N-terminal region but an overall β-propeller-like fold, and CD spectra reveal nearly exclusively β-sheet secondary structure in solution[31]. Given that many different globular proteins can form a diversity of amyloid fibril structures[57; 86], it will be interesting to clarify the amyloidogenic region(s). Our truncation fusion constructs support the notion that fibril formation ensues from multiple peptide segments in different regions of the ~30 kDa protein; there many not be a clear domain responsible for fibril formation, as seen for example, in the yeast prion sup35[87]. In addition, the current lack of evidence for multiple smaller domains within OLF[31] indicates that the native folding pathway for myoc-OLF may be quite complex and prone to populating aggregation-prone intermediates[88]. Once conditions for reversible unfolding have been found, any commonalities in the accumulated intermediate(s) among the ~70 glaucoma-causing OLF variants can be explored in detail. Of particular interest is the folding pathway of disease-causing variants with WT-like stability, which still produce MBP-OLF aggregates at a higher level than for wild-type[15]. In sum, aside from the tantalizing possibility of pathological relevance for myoc-OLF amyloid fibrils, the myriad open molecular biophysical questions surrounding OLF molecular structure, folding pathways, and function, will be captivating for further study.

Materials and Methods

Protein Expression and Purification

The plasmid for MBP-OLF with a Factor Xa cleavage site was cloned as described previously[20; 31]. Myoc-OLF mutants and truncated forms of MBP-OLF were generated by site-directed mutagenesis (QuikChange, Stratagene) of the MBP-OLF encoded plasmid. All plasmids were verified by DNA sequencing (MWG Operon). Cell culture and protein expression in E. coli Rosetta-Gami 2(DE3)pLysS cells (Novagen), and purification were carried out as described previously[20; 31]. Briefly, cells were lysed by French Press, ultracentrifuged at 100,000 × g to remove all insoluble material, and the supernatant was purified over an amylose affinity column using an Akta FPLC system (GE Healthcare). The purified material was further subjected to SEC (Superdex 75 pg or GL, GE Healthcare) to identify oligomeric state(s) of the construct of interest. Cleavage of myoc-OLF from MBP was accomplished by incubating with Factor Xa (Roche or NEB Biolabs) and additional chromatographic steps to remove all traces of MBP, as described previously[20; 31]. The use of tandem Akta FPLC instruments ensured that protein purification was completed within one week.

ThT Binding

As a tinctorial indicator for the presence of mature amyloid fibrils, binding of ThT to various constructs of interest (30 μM) was confirmed by monitoring the fluorescence intensity using a RF-5301 PC spectrofluorophotometer (Shimadzu) after 1 min incubation with 5 μM ThT (Ex λ: 440 nm; Em λ: 485 nm). Phosphate buffered saline (PBS, 10 mM

Na_2H/KH_2PO_4, 200 mM NaCl, pH 7.2) concentration was controlled for by diluting a 5X stock. All spectra were blank-subtracted. All ThT binding experiments were conducted under identical conditions except where noted in at least duplicate.

In vitro Fibril Formation

Monomeric myoc-OLF (30 μM) in PBS was incubated in the presence of various destabilizing agents at 37 °C for 24-95 hr including SDS (0-10 mM), H_2O_2 (0-2.9%), The SDS samples were incubated in a dry incubator, whereas samples incubated in peroxide conditions were incubated in a circulating water bath. The presence of amyloid fibrils was assessed by ThT fluorescence (above), EM, and CD, as described in the text.

Spontaneous and Seeded Aggregation Assays

Spontaneous fibril formation of myoc-OLF without the addition of SDS or other destabilizing reagent was conducted by incubating ~30 μM myoc-OLF in PBS placed on a two-dimensional rocker in a 37 °C dry incubator. For each time point, an aliquot was removed for ThT fluorescence measurements, as above. In the case of myoc-OLF(Y437H), 30 μM of protein with 5 μM ThT were incubated in a 37 °C circulating water bath and fluorescence reading taken at hourly intervals. For the seeding assays, preformed myoc-OLF fibrils (0.5 mM SDS, 37 °C incubation in a water bath overnight) were pelleted at ~4000 × g and washed in PBS to remove the SDS. To fragment the fibrils, 20 pulses at a 20% duty cycle using a sonicator (Branson Sonifier 450) were applied. Monomeric myoc-OLF was inoculated with 15 μM, or, only in the case of myoc-OLF, 30 μM seeds in a 100 μL reaction volume in with PBS, 0.5 mM SDS, and 40 μM ThT. For myoc-OLF(Y437H), the procedure differed from that of myoc-OLF in that protein and seed concentration were both 15 μM. Fluorescence intensity was monitored as described above while the sample incubated at 30 °C in a circulating water bath. In the case of the multiple round seeding assays, myoc-OLF fibrils of the previous round were used as seeds for the next round using a 1:1 ratio seeds to monomer (15 μM each). Fibril formation was followed by increase in ThT fluorescence, as above.

Proteinase K Digestion

Proteinase K digestion was carried out similar to a protocol described before[34]. In short, proteinase K (1.2 U, NEB) was added to 2 mL of 8 μM MBP-OLF fibrils diluted in reaction buffer (50 mM Tris HCl, pH 8.0 and 150 mM NaCl) and incubated for 1 hr in a 37 °C water bath. The reaction was then purified by amylose affinity resin, and the unbound flowthrough fractions were subjected to SEC using Superdex 75 pg. The elution fractions corresponding to the void volume were concentrated using filtration device and analyzed by ThT fluorescence as described above and by Tricine-SDS-PAGE (16%/ 6 M urea separating gel, 10% spacer gel, and 4% stacking gel)[89].

Circular Dichroism

Circular dichroism spectra were acquired was performed on a Jasco J-810 spectopolarimeter. 13 μM preformed myoc-OLF fibrils (0.5 mM SDS, 37 °C incubation in a water bath overnight) was prepared in PBS. The profiles were monitored between 200 and 300 nm in a 0.1 cm cell. Ten spectra were scanned for each sample at a scan rate of 500 nm min^{-1} and were then averaged. The averaged spectrum was background-corrected and converted to mean residue ellipticity $[\Theta] = M_{res} \times \Theta_{obs}/10 \times d \times c$, where $M_{res} = 112.9$ is the mean residue ellipticity calculated from the protein sequence; Θ_{obs} is the observed ellipticity (degrees) at wavelength λ; d is the pathlength (cm); and c is the protein concentration (g/mL).

Identification of Prefibrillar Oligomers by the Conformationally Specific Antibody A11

For MBP-OLF derived samples, 2 μL of 1 μM protein was spotted onto a pre-wet PVDF membrane (Bio-Rad) and allowed to air dry. The membranes were blocked in 10% non-fat milk for one hour followed by a washing step and subsequent incubation in either the oligomer-specific A11 (0.5 μg/mL, Invitrogen) or anti-MBP (0.2 μg/mL, NEB) primary antibodies for one hour. The membranes were then washed and incubated with anti-rabbit IgG conjugated with horseradish peroxidase (HRP) (0.1 μg/mL, AnaSpec) for one hour. The blots were developed with chemiluminescent HRP detection reagent (Denville). For PK-treated samples, 0.5 μg of total protein was blotted using A11 in a similar manner.

Transmission Electron Microscopy

Samples containing aggregated material were visualized by transmission electron microscopy. Sample volumes of 2 uL were pipetted onto carbon-coated 400-mesh copper grids and blotted after 1 min with Whatman #4 filter paper. Immediately after blotting, a 2 uL aliquot of 1% uranyl acetate was added to the grid and again blotted after 30 s. Images of negatively stained samples were collected with a JEOL JEM-1400 transmission electron microscope. Samples were screened at low magnification with an Orius SC1000 CCD camera and any samples exhibiting bacterial contamination were eliminated from further analysis. Once fibrils were identified, images were collected with an UltraScan1000 CCD camera at a magnification of 20,000x – 30,000x.

Creation of Stable Cell Lines with Tetracycline Inducible Myocilin Expression

To place myocilin cDNAs under the control of a tetracycline-inducible promoter, DNA fragments encoding wild type or P370L mutant myocilin fused at the 3′ end with a sequence encoding the 15 amino acid S-peptide tag[90] were inserted into the *PmeI* site of pcDNA4/TO (Invitrogen). DNA sequence analysis was performed to confirm that coding sequences were correct and in-frame with the S-peptide tag. To create stable cell lines with inducible myocilin expression, plasmids pcDNA4/TO-Myoc WT-S-tag and pcDNA4/TO-Myoc P370L-S-tag and the vector pcDNA4/TO control were individually transfected into T-REX-CHO cells (Invitrogen) using Lipofectamine plus (Invitrogen). Two days after transfection, 50 μg/mL zeocin was added to select transfectants. Single cell colonies were picked following selection with zeocin (Invitrogen) for about two weeks. The expression of recombinant myocilin protein was induced by adding 1μg/mL tetracycline (Invitrogen) and verified by immunoblot at 48 hr post-induction. Cloned cell lines were designated T-REX-CHO (pcDNA4/TO-Myoc-WT-S-tag), T-REX-CHO (pcDNA4/TO-Myoc-P370L-S-tag) and T-REX-CHO (pcDNA4/TO vector). For experiments, stable inducible cells were grown in Ham's F12 medium (Cellgro) supplemented with 5% FBS (Invitrogen), 1% penicillin-streptomycin (Invitrogen), 2 mM glutamine (Invitrogen), 10 μg/mL blasticidin (Invitrogen), and 50 μg/mL zeocin.

In-cell ThT Staining

Overnight, 6×10^4 cells were grown on poly-D-lysine-coated cover slips and the expression of myocilin was then induced by adding 1 μg/ml tetracycline for 48 hr. Cells were processed for ThT staining essentially as described[54]. Briefly, cells were fixed in 4% paraformaldehyde at room temperature for 15 min and washed in PBS three times. Cells were stained with Mayer's hematoxylin for 2 min, washed in water for 5 min, then incubated in 1% (w/v) ThT for 3 min, rinsed in water again for 5 min, and finally incubated in 1% (v/v) acetic acid for 20 min. After the stained cells were washed thoroughly in water, cover slips were mounted with FluorSave Reagent (Calbiochem) for 2 hr. Fluorescence microscopy was used to identify and quantify ThT positive cells, which appeared green.

Triton X-100 Extraction and Boiled Gel Analysis

Cell pellets from pcDNA4/TO-Myoc-WT-S-tag, pcDNA4/TO-Myoc-P370L-S-tag, and pcDNA4/TO expression were thawed from −80 °C on ice, resuspended in 400 μL of extraction buffer (1X PBS, pH 7.4, 5 mM EDTA, 1% Triton X-100 (TX) with Complete protease inhibitor cocktail (Roche)), incubated on ice for 30 minutes, and centrifuged at ~13,000 g for 15 minutes. The supernatant was then transferred to a new microcentrifuge tube and set aside as the TX-soluble fraction. The pellet, the TX-insoluble fraction, as solubilized in 100 μL of SDS buffer (1% SDS in PBS) for 10 minutes at room temperature. After addition of 300 μL extraction buffer, the sample was sonicated for 20 s using a 50% duty cycle.

The boiled-gel protocol was adapted from a protocol for purification of yeast prion polymers from cell lysates[55]. In brief, a loading dye containing 1% SDS was added to TX-soluble and TX-insoluble samples of CHO-cell derived myocilin (40 μg total protein). Samples were loaded without boiling and subjected to SDS-PAGE for 45 minutes. The electrophoresis step was halted and the wells for one gel were sealed upon polymerization of a new aliquot of stacking gel. This sealed gel was incubated over a boiling water bath for 10 minutes, cooled to room temperature, and then subjected to a second electrophoresis step for an additional hour. Material from gels were transferred to Immun-Blot PVDF membrane (Bio-Rad) and probed by Western Blot using anti-S-tag primary antibody (S-probe (K-14), Santa Cruz Biotechnology) and visualized by chemiluminescence.

Supplementary Material

Refer to Web version on PubMed Central for supplementary material.

Acknowledgments

This work was supported by grants from the NIH (R01EY021205), the American Health Assistance Foundation, the Blanchard Foundation, and Pew Foundation to RLL, and from the NIH (R01EY011405) and The Glaucoma Foundation to DV. SDO was supported in part by United States Department of Education Graduate Assistance in Areas of National Need program P200A060188, and CWP by the Beckman Scholars Program. We thank Rebecca Donegan, Dr. Tanay Desai, and Pamela Chi for assistance with sample preparation and data analysis, as well as Yury Chernoff and Andrey Romanyuk for advice and helpful discussions.

Abbreviations

TM	trabecular meshwork
WT	wild-type
OLF	olfactomedin
IOP	intraocular pressure
ER	endoplasmic reticulum
ERAD	ER associated degradation
MBP	maltose-binding protein
SEC	size exclusion chromatography
SDS-PAGE	sodium dodecyl sulfate – polyacrylamide gel electrophoresis
CD	circular dichroism
ThT	thioflavin T

PK	proteinase K
EM	electron microscopy
Aβ	amyloid-β
TX	Triton X-100
CHO	Chinese Hamster Ovary
PBS	phosphate-buffered saline.

References

1. Kwon YH, Fingert JH, Kuehn MH, Alward WL. Primary open-angle glaucoma. N. Engl. J. Med. 2009; 360:1113–24. [PubMed: 19279343]
2. Alward WL. Medical management of glaucoma. N. Engl. J. Med. 1998; 339:1298–307. [PubMed: 9791148]
3. Gasiorowski J, Russell P. Biological properties of trabecular meshwork cells. Exp. Eye Res. 2009; 88:671–675. [PubMed: 18789927]
4. Kass MA, Heuer DK, Higginbotham EJ, Johnson CA, Keltner JL, Miller JP, Parrish RK, Wilson MR, Gordon MO. The Ocular Hypertension Treatment Study: a randomized trial determines that topical ocular hypotensive medication delays or prevents the onset of primary open-angle glaucoma. Archives of Ophthalmology. 2002; 120:701–13. discussion 829-30. [PubMed: 12049574]
5. Resch Z, Fautsch M. Glaucoma-associated myocilin: A better understanding but much more to learn. Exp. Eye Res. 2009; 88:704–12. [PubMed: 18804106]
6. Gong G, Kosoko-Lasaki O, Haynatzki GR, Wilson MR. Genetic dissection of myocilin glaucoma. Hum. Mol. Genet. 2004; 13:R91–102. [PubMed: 14764620]
7. Zhou Z, Vollrath D. A cellular assay distinguishes normal and mutant TIGR/myocilin protein. Hum. Mol. Genet. 1999; 8:2221–8. [PubMed: 10545602]
8. Shepard AR, Jacobson N, Millar JC, Pang I-H, Steely HT, Searby CC, Sheffield VC, Stone EM, Clark AF. Glaucoma-causing myocilin mutants require the Peroxisomal targeting signal-1 receptor (PTS1R) to elevate intraocular pressure. Human Molecular Genetics. 2006; 16:609–617. [PubMed: 17317787]
9. Liu Y, Vollrath D. Reversal of mutant myocilin non-secretion and cell killing: implications for glaucoma. Hum. Mol. Genet. 2004; 13:1193–204. [PubMed: 15069026]
10. Zhou Y, Grinchuk O, Tomarev SI. Transgenic mice expressing the Tyr437His mutant of human myocilin protein develop glaucoma. Invest. Ophthalmol. Vis. Sci. 2008; 49:1932–9. [PubMed: 18436825]
11. Senatorov V, Malyukova I, Fariss R, Wawrousek EF, Swaminathan S, Sharan SK, Tomarev S. Expression of mutated mouse myocilin induces open-angle glaucoma in transgenic mice. J. Neurosci. 2006; 26:11903–14. [PubMed: 17108164]
12. Wang L, Zhuo Y, Liu B, Huang S, Hou F, Ge J. Pro370Leu mutant myocilin disturbs the endoplasm reticulum stress response and mitochondrial membrane potential in human trabecular meshwork cells. Mol. Vis. 2007; 13:618–25. [PubMed: 17515882]
13. Joe MK, Sohn S, Hur W, Moon Y, Choi YR, Kee C. Accumulation of mutant myocilins in ER leads to ER stress and potential cytotoxicity in human trabecular meshwork cells. Biochem. Biophys. Res. Commun. 2003; 312:592–600. [PubMed: 14680806]
14. Yam GH-F, Gaplovska-Kysela K, Zuber C, Roth J. Aggregated myocilin induces russell bodies and causes apoptosis: implications for the pathogenesis of myocilin-caused primary open-angle glaucoma. Am. J. Pathol. 2007; 170:100–9. [PubMed: 17200186]
15. Burns JN, Turnage KC, Walker CA, Lieberman RL. The stability of myocilin olfactomedin domain variants provides new insight into glaucoma as a protein misfolding disorder. Biochemistry. 2011; 50:5824–33. [PubMed: 21612213]

16. Vembar SS, Brodsky JL. One step at a time: endoplasmic reticulum-associated degradation. Nat. Rev. Mol. Cell Biol. 2008; 9:944–57. [PubMed: 19002207]

17. Gobeil S, Rodrigue M-A, Moisan S, Nguyen TD, Polansky JR, Morissette J, Raymond V. Intracellular sequestration of hetero-oligomers formed by wild-type and glaucoma-causing myocilin mutants. Invest. Ophthalmol. Vis. Sci. 2004; 45:3560–7. [PubMed: 15452063]

18. Lam DS, Leung YF, Chua JK, Baum L, Fan DS, Choy KW, Pang CP. Truncations in the TIGR gene in individuals with and without primary open-angle glaucoma. Invest. Ophthalmol. Vis. Sci. 2000; 41:1386–91. [PubMed: 10798654]

19. Kim BS, Savinova OV, Reedy MV, Martin J, Lun Y, Gan L, Smith RS, Tomarev SI, John SW, Johnson RL. Targeted disruption of the myocilin gene (myoc) suggests that human glaucoma-causing mutations are gain of function. Mol. Cell. Biol. 2001; 21:7707–13. [PubMed: 11604506]

20. Burns JN, Orwig SD, Harris JL, Watkins JD, Vollrath D, Lieberman RL. Rescue of glaucoma-causing mutant myocilin thermal stability by chemical chaperones. ACS Chem. Biol. 2010; 5:477–87. [PubMed: 20334347]

21. Yam GH-F, Gaplovska-Kysela K, Zuber C, Roth J. Sodium 4-phenylbutyrate acts as a chemical chaperone on misfolded myocilin to rescue cells from endoplasmic reticulum stress and apoptosis. Invest. Ophthalmol. Vis. Sci. 2007; 48:1683–90. [PubMed: 17389500]

22. Jia L-Y, Gong B, Pang C-P, Huang Y, Lam DS-C, Wang N, Yam GH-F. Correction of the disease phenotype of myocilin-causing glaucoma by a natural osmolyte. Invest. Ophthalmol. Vis. Sci. 2009; 50:3743–9. [PubMed: 19234343]

23. Zode GS, Kuehn MH, Nishimura DY, Searby CC, Mohan K, Grozdanic SD, Bugge K, Anderson MG, Clark AF, Stone EM, Sheffield VC. Reduction of ER stress via a chemical chaperone prevents disease phenotypes in a mouse model of primary open angle glaucoma. J. Clin. Invest. 2011; 121:3542–53. [PubMed: 21821918]

24. Nakano M, Ikeda Y, Taniguchi T, Yagi T, Fuwa M, Omi N, Tokuda Y, Tanaka M, Yoshii K, Kageyama M, Naruse S, Matsuda A, Mori K, Kinoshita S, Tashiro K. Three susceptible loci associated with primary open-angle glaucoma identified by genome-wide association study in a Japanese population. Proc Natl Acad Sci USA. 2009; 106:12838–42. [PubMed: 19625618]

25. Wordinger RJ, Clark AF. Effects of glucocorticoids on the trabecular meshwork: towards a better understanding of glaucoma. Prog. Retin. Eye Res. 1999; 18:629–67. [PubMed: 10438153]

26. Polansky JR, Fauss DJ, Chen P, Chen H, Lutjen-Drecoll E, Johnson D, Kurtz RM, Ma ZD, Bloom E, Nguyen TD. Cellular pharmacology and molecular biology of the trabecular meshwork inducible glucocorticoid response gene product. Ophthalmologica. 1997; 211:126–39. [PubMed: 9176893]

27. Carbone MA, Ayroles JF, Yamamoto A, Morozova TV, West SA, Magwire MM, Mackay TFC, Anholt RRH. Overexpression of myocilin in the Drosophila eye activates the unfolded protein response: implications for glaucoma. PLoS ONE. 2009; 4:e4216. [PubMed: 19148291]

28. Tamm ER, Ethier CR. Current aspects of aqueous humor dynamics and glaucoma. Exp. Eye. Res. 2009; 88:618–9. [PubMed: 19250933]

29. Stone EM, Fingert JH, Alward WL, Nguyen TD, Polansky JR, Sunden SL, Nishimura D, Clark AF, Nystuen A, Nichols BE, Mackey DA, Ritch R, Kalenak JW, Craven ER, Sheffield VC. Identification of a gene that causes primary open angle glaucoma. Science. 1997; 275:668–70. [PubMed: 9005853]

30. Shimizu S, Lichter PR, Johnson AT, Zhou Z, Higashi M, Gottfredsdottir M, Othman M, Moroi SE, Rozsa FW, Schertzer RM, Clarke MS, Schwartz AL, Downs CA, Vollrath D, Richards JE. Age-dependent prevalence of mutations at the GLC1A locus in primary open-angle glaucoma. Am. J. Ophthalmol. 2000; 130:165–77. [PubMed: 11004290]

31. Orwig SD, Lieberman RL. Biophysical characterization of the olfactomedin domain of myocilin, an extracellular matrix protein implicated in inherited forms of glaucoma. PLoS ONE. 2011; 6:e16347. [PubMed: 21283635]

32. Goldschmidt L, Teng PK, Riek R, Eisenberg D. Identifying the amylome, proteins capable of forming amyloid-like fibrils. Proc. Natl. Acad. Sci. U S A. 2010; 107:3487–92. [PubMed: 20133726]

33. LeVine H 3rd. Quantification of beta-sheet amyloid fibril structures with thioflavin T. Methods Enzymol. 1999; 309:274–84. [PubMed: 10507030]
34. Balguerie A, Dos Reis S, Ritter C, Chaignepain S, Coulary-Salin B, Forge V, Bathany K, Lascu I, Schmitter JM, Riek R, Saupe SJ. Domain organization and structure-function relationship of the HET-s prion protein of Podospora anserina. EMBO J. 2003; 22:2071–81. [PubMed: 12727874]
35. Caughey BW, Dong A, Bhat KS, Ernst D, Hayes SF, Caughey WS. Secondary structure analysis of the scrapie-associated protein PrP 27-30 in water by infrared spectroscopy. Biochemistry. 1991; 30:7672–80. [PubMed: 1678278]
36. Shirahama T, Cohen AS. High-resolution electron microscopic analysis of the amyloid fibril. J. Cell Biol. 1967; 33:679–708. [PubMed: 6036530]
37. Hardy J, Selkoe DJ. The amyloid hypothesis of Alzheimer's disease: progress and problems on the road to therapeutics. Science. 2002; 297:353–6. [PubMed: 12130773]
38. Walsh DM, Hartley DM, Kusumoto Y, Fezoui Y, Condron MM, Lomakin A, Benedek GB, Selkoe DJ, Teplow DB. Amyloid beta-protein fibrillogenesis. Structure and biological activity of protofibrillar intermediates. J. Biol. Chem. 1999; 274:25945–52. [PubMed: 10464339]
39. Lashuel HA, Hartley D, Petre BM, Walz T, Lansbury PT Jr. Neurodegenerative disease: amyloid pores from pathogenic mutations. Nature. 2002; 418:291. [PubMed: 12124613]
40. Kayed R, Head E, Thompson JL, McIntire TM, Milton SC, Cotman CW, Glabe CG. Common structure of soluble amyloid oligomers implies common mechanism of pathogenesis. Science. 2003; 300:486–9. [PubMed: 12702875]
41. Kapust RB, Waugh DS. Escherichia coli maltose-binding protein is uncommonly effective at promoting the solubility of polypeptides to which it is fused. Protein Sci. 1999; 8:1668–74. [PubMed: 10452611]
42. Novokhatny V, Ingham K. Thermodynamics of maltose binding protein unfolding. Protein Sci. 1997; 6:141–6. [PubMed: 9007986]
43. Ganesh C, Zaidi FN, Udgaonkar JB, Varadarajan R. Reversible formation of on-pathway macroscopic aggregates during the folding of maltose binding protein. Protein Sci. 2001; 10:1635–44. [PubMed: 11468360]
44. de Groot NS, Sabate R, Ventura S. Amyloids in bacterial inclusion bodies. Trends Biochem. Sci. 2009; 34:408–16. [PubMed: 19647433]
45. Naiki H, Higuchi K, Nakakuki K, Takeda T. Kinetic analysis of amyloid fibril polymerization in vitro. Lab. Invest. 1991; 65:104–10. [PubMed: 1906561]
46. Naiki H, Nakakuki K. First-order kinetic model of Alzheimer's beta-amyloid fibril extension in vitro. Lab. Invest. 1996; 74:374–83. [PubMed: 8780157]
47. Yamamoto S, Hasegawa K, Yamaguchi I, Tsutsumi S, Kardos J, Goto Y, Gejyo F, Naiki H. Low concentrations of sodium dodecyl sulfate induce the extension of beta 2-microglobulin-related amyloid fibrils at a neutral pH. Biochemistry. 2004; 43:11075–82. [PubMed: 15323566]
48. Giehm L, Oliveira CL, Christiansen G, Pedersen JS, Otzen DE. SDS-induced fibrillation of alpha-synuclein: an alternative fibrillation pathway. J. Mol. Biol. 2010; 401:115–33. [PubMed: 20540950]
49. Necula M, Chirita CN, Kuret J. Rapid anionic micelle-mediated alpha-synuclein fibrillization in vitro. J. Biol. Chem. 2003; 278:46674–80. [PubMed: 14506232]
50. Conway KA, Harper JD, Lansbury PT Jr. Fibrils formed in vitro from alpha-synuclein and two mutant forms linked to Parkinson's disease are typical amyloid. Biochemistry. 2000; 39:2552–63. [PubMed: 10704204]
51. Jaikaran ET, Higham CE, Serpell LC, Zurdo J, Gross M, Clark A, Fraser PE. Identification of a novel human islet amyloid polypeptide beta-sheet domain and factors influencing fibrillogenesis. J. Mol. Biol. 2001; 308:515–25. [PubMed: 11327784]
52. Sacca SC, Bolognesi C, Battistella A, Bagnis A, Izzotti A. Gene-environment interactions in ocular diseases. Mutat Res. 2009; 667:98–117. [PubMed: 19046976]
53. Ghanem AA, Arafa LF, El-Baz A. Oxidative stress markers in patients with primary open-angle glaucoma. Curr. Eye Res. 2010; 35:295–301. [PubMed: 20373896]
54. Westermark GT, Johnson KH, Westermark P. Staining methods for identification of amyloid in tissue. Methods Enzymol. 1999; 309:3–25. [PubMed: 10507013]

55. Kushnirov VV, Alexandrov IM, Mitkevich OV, Shkundina IS, Ter-Avanesyan MD. Purification and analysis of prion and amyloid aggregates. Methods. 2006; 39:50–5. [PubMed: 16774835]
56. Hartley DM, Walsh DM, Ye CP, Diehl T, Vasquez S, Vassilev PM, Teplow DB, Selkoe DJ. Protofibrillar intermediates of amyloid beta-protein induce acute electrophysiological changes and progressive neurotoxicity in cortical neurons. J. Neurosci. 1999; 19:8876–84. [PubMed: 10516307]
57. Eichner T, Radford SE. A diversity of assembly mechanisms of a generic amyloid fold. Mol. Cell. 2011; 43:8–18. [PubMed: 21726806]
58. Surguchev A, Surguchov A. Conformational diseases: looking into the eyes. Brain Res. Bull. 2010; 81:12–24. [PubMed: 19808079]
59. McKinnon SJ, Lehman DM, Kerrigan-Baumrind LA, Merges CA, Pease ME, Kerrigan DF, Ransom NL, Tahzib NG, Reitsamer HA, Levkovitch-Verbin H, Quigley HA, Zack DJ. Caspase activation and amyloid precursor protein cleavage in rat ocular hypertension. Invest. Ophthalmol. Vis. Sci. 2002; 43:1077–87. [PubMed: 11923249]
60. Guo L, Salt TE, Luong V, Wood N, Cheung W, Maass A, Ferrari G, Russo-Marie F, Sillito AM, Cheetham ME, Moss SE, Fitzke FW, Cordeiro MF. Targeting amyloid-beta in glaucoma treatment. Proc Natl Acad Sci U S A. 2007; 104:13444–9. [PubMed: 17684098]
61. Yoneda S, Hara H, Hirata A, Fukushima M, Inomata Y, Tanihara H. Vitreous fluid levels of beta-amyloid((1-42)) and tau in patients with retinal diseases. Jpn. J. Ophthalmol. 2005; 49:106–8. [PubMed: 15838725]
62. Head MW, Northcott V, Rennison K, Ritchie D, McCardle L, Bunn TJ, McLennan NF, Ironside JW, Tullo AB, Bonshek RE. Prion protein accumulation in eyes of patients with sporadic and variant Creutzfeldt-Jakob disease. Invest. Ophthalmol. Vis. Sci. 2003; 44:342–6. [PubMed: 12506094]
63. Gabelt BAT, Kaufman PL. Changes in aqueous humor dynamics with age and glaucoma. Progress in retinal and eye research. 2005; 24:612–37. [PubMed: 15919228]
64. Tomarev SI, Wistow G, Raymond V, Dubois S, Malyukova I. Gene expression profile of the human trabecular meshwork: NEIBank sequence tag analysis. Invest. Ophthalmol. Vis. Sci. 2003; 44:2588–96. [PubMed: 12766061]
65. Ueda J, Wentz-Hunter KK, Cheng EL, Fukuchi T, Abe H, Yue BY. Ultrastructural localization of myocilin in human trabecular meshwork cells and tissues. J. Histochem. Cytochem. 2000; 48:1321–30. [PubMed: 10990486]
66. Ueda J, Wentz-Hunter K, Yue BY. Distribution of myocilin and extracellular matrix components in the juxtacanalicular tissue of human eyes. Invest. Ophthalmol. Vis. Sci. 2002; 43:1068–76. [PubMed: 11923248]
67. Filla MS, Liu X, Nguyen TD, Polansky JR, Brandt CR, Kaufman PL, Peters DM. In vitro localization of TIGR/MYOC in trabecular meshwork extracellular matrix and binding to fibronectin. Invest. Ophthalmol. Vis. Sci. 2002; 43:151–61. [PubMed: 11773026]
68. Tektas OY, Lutjen-Drecoll E. Structural changes of the trabecular meshwork in different kinds of glaucoma. Exp. Eye Res. 2009; 88:769–75. [PubMed: 19114037]
69. Relini A, Canale C, De Stefano S, Rolandi R, Giorgetti S, Stoppini M, Rossi A, Fogolari F, Corazza A, Esposito G, Gliozzi A, Bellotti V. Collagen plays an active role in the aggregation of beta2-microglobulin under physiopathological conditions of dialysis-related amyloidosis. J. Biol. Chem. 2006; 281:16521–9. [PubMed: 16601119]
70. Alexandrescu AT. Amyloid accomplices and enforcers. Protein Sci. 2005; 14:1–12. [PubMed: 15576561]
71. Solomon JP, Bourgault S, Powers ET, Kelly JW. Heparin binds 8 kDa gelsolin cross-beta-sheet oligomers and accelerates amyloidogenesis by hastening fibril extension. Biochemistry. 2011; 50:2486–98. [PubMed: 21348501]
72. McLaurin J, Franklin T, Zhang X, Deng J, Fraser PE. Interactions of Alzheimer amyloid-beta peptides with glycosaminoglycans effects on fibril nucleation and growth. Eur. J. Biochem. 1999; 266:1101–10. [PubMed: 10583407]
73. Relini A, De Stefano S, Torrassa S, Cavalleri O, Rolandi R, Gliozzi A, Giorgetti S, Raimondi S, Marchese L, Verga L, Rossi A, Stoppini M, Bellotti V. Heparin strongly enhances the formation of

beta2-microglobulin amyloid fibrils in the presence of type I collagen. J. Biol. Chem. 2008; 283:4912–20. [PubMed: 18056266]

74. Bence NF, Sampat RM, Kopito RR. Impairment of the ubiquitin-proteasome system by protein aggregation. Science. 2001; 292:1552–5. [PubMed: 11375494]
75. Mertts M, Garfield S, Tanemoto K, Tomarev SI. Identification of the region in the N-terminal domain responsible for the cytoplasmic localization of Myoc/Tigr and its association with microtubules. Lab. Invest. 1999; 79:1237–45. [PubMed: 10532587]
76. Resch ZT, Hann CR, Cook KA, Fautsch MP. Aqueous humor rapidly stimulates myocilin secretion from human trabecular meshwork cells. Exp. Eye Res. 2010; 91:901–8. [PubMed: 20932969]
77. Hardy KM, Hoffman EA, Gonzalez P, McKay BS, Stamer WD. Extracellular trafficking of myocilin in human trabecular meshwork cells. J. Biol. Chem. 2005; 280:28917–26. [PubMed: 15944158]
78. Stamer W, Perkumas K, Hoffman E. Coiled-coil targeting of myocilin to intracellular membranes. Experimental Eye Research. 2006
79. Liton PB, Lin Y, Gonzalez P, Epstein DL. Potential role of lysosomal dysfunction in the pathogenesis of primary open angle glaucoma. Autophagy. 2009; 5:122–4. [PubMed: 19001861]
80. Tomarev SI, Nakaya N. Olfactomedin domain-containing proteins: possible mechanisms of action and functions in normal development and pathology. Mol. Neurobiol. 2009; 40:122–38. [PubMed: 19554483]
81. Snyder DA, Rivers AM, Yokoe H, Menco BP, Anholt RR. Olfactomedin: purification, characterization, and localization of a novel olfactory glycoprotein. Biochemistry. 1991; 30:9143–53. [PubMed: 1892825]
82. Hillier BJ, Vacquier VD. Structural features and functional domains of amassin-1, a cell-binding olfactomedin protein. Biochem. Cell Biol. 2007; 85:552–562. [PubMed: 17901897]
83. Goldwich A, Scholz M, Tamm ER. Myocilin promotes substrate adhesion, spreading and formation of focal contacts in podocytes and mesangial cells. Histochem. Cell Biol. 2009; 131:167–80. [PubMed: 18855004]
84. Yu L, Wang L, Chen S. Olfactomedin 4, a novel marker for the differentiation and progression of gastrointestinal cancers. Neoplasma. 2011; 58:9–13. [PubMed: 21067260]
85. Kim DE, Chivian D, Baker D. Protein structure prediction and analysis using the Robetta server. Nucleic Acids Res. 2004; 32:W526–31. [PubMed: 15215442]
86. Toyama BH, Weissman JS. Amyloid structure: conformational diversity and consequences. Annu. Rev. Biochem. 2011; 80:557–85. [PubMed: 21456964]
87. Paushkin SV, Kushnirov VV, Smirnov VN, Ter-Avanesyan MD. In vitro propagation of the prion-like state of yeast Sup35 protein. Science. 1997; 277:381–3. [PubMed: 9219697]
88. Jahn TR, Radford SE. Folding versus aggregation: polypeptide conformations on competing pathways. Arch. Biochem. Biophys. 2008; 469:100–17. [PubMed: 17588526]
89. Schagger H. Tricine-SDS-PAGE. Nat. Protoc. 2006; 1:16–22. [PubMed: 17406207]
90. Kim JS, Raines RT. Ribonuclease S-peptide as a carrier in fusion proteins. Protein Sci. 1993; 2:348–56. [PubMed: 8453373]

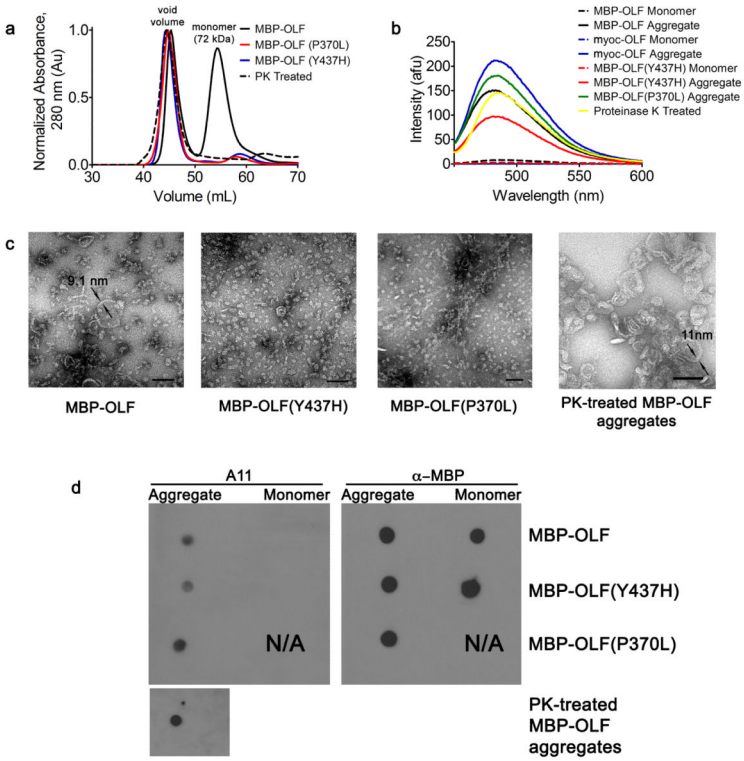

Figure 1.

MBP-OLF fibrils and pre-fibrillar oligomers isolated from *E. coli*. (a) Overlay of Superdex 75 chromatographs from WT MBP-OLF, MBP-OLF(P370L), MBP-OLF(Y437H), and PK-treated MBP-OLF. (b) Corresponding ThT fluorescence of monomeric and aggregate MBP-OLF variants, as well as de novo formed myoc-OLF fibrils (asterisk, see text). (c) Micrographs of aggregates isolated in (a). Scale bar = 100 nm with two measured fibril widths indicated. (d) Detection of protofibillar oligomers in aggregates isolated in (a) using the A11 antibody. Anti-MBP used as a positive control where possible.

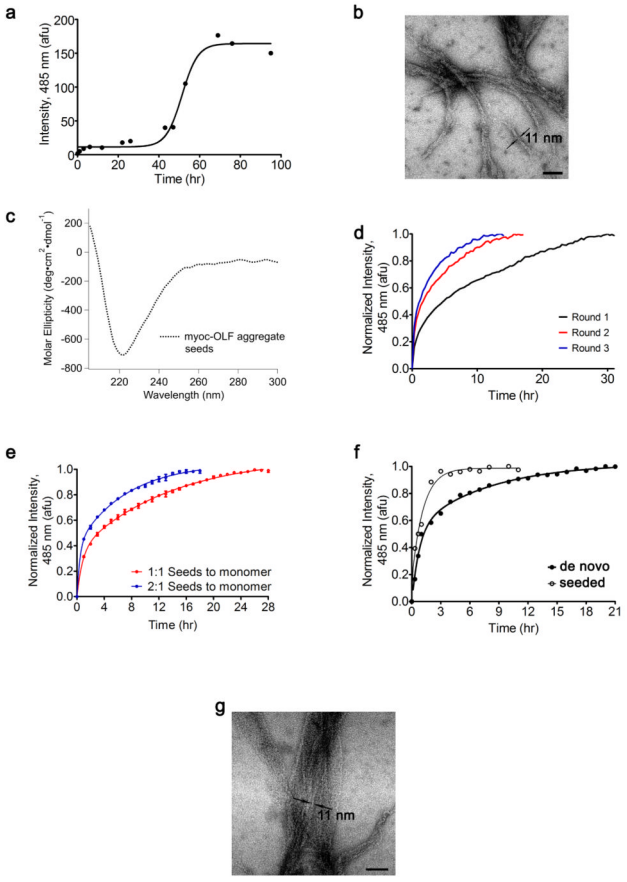

Figure 2.

De novo and seeded fibril formation of myoc-OLF. (a) Representative nucleation-dependent fibrillization of myoc-OLF incubated at 37 °C monitored by ThT fluorescence. (b) Micrograph of de novo formed myoc-OLF fibrils generated in the same procedure as in (a). Scale bar = 100 nm with measured fibril width indicated (c) CD spectrum of myoc-OLF in vitro fibrils prepared by overnight incubation at 37 °C with 0.5 mM SDS (see text). (d) Representative multiple-round seeding kinetics with myoc-OLF. (e) Seeding kinetics with different quantities of seeds. (f) Representative de novo fibril formation of myoc-OLF(Y437H) and fibril formation initiated with WT myoc-OLF seeds. (g) Micrograph after treatment of myoc-OLF with 1.5% H_2O_2 incubated at 37 °C.

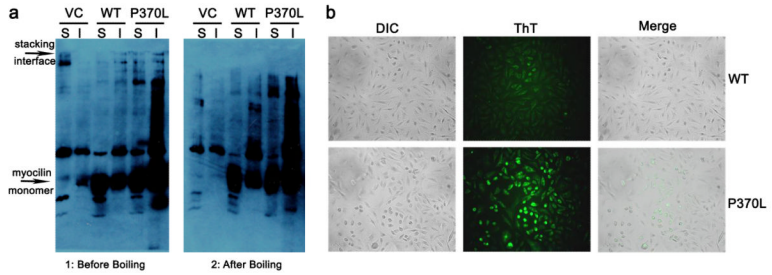

Figure 3.

Myocilin fibrils isolated from CHO cells. (a) Gel mobility of Triton X-100 soluble and insoluble isolates from vector control (VC), WT myocilin, and myocilin(P370L). Left: gel without boiling. Accumulation of material appears at the stacking interface. Right: gel after steaming. Accumulated protein from stacking interface has entered the resolving gel. S = soluble, I = insoluble fraction, as designated by TX-100 fractionation. (b) In-cell ThT fluorescence of WT and P370L variants of myocilin. Overlay of differential interference contrast (DIC) and ThT fluorescence confirm intracellular aggregation.

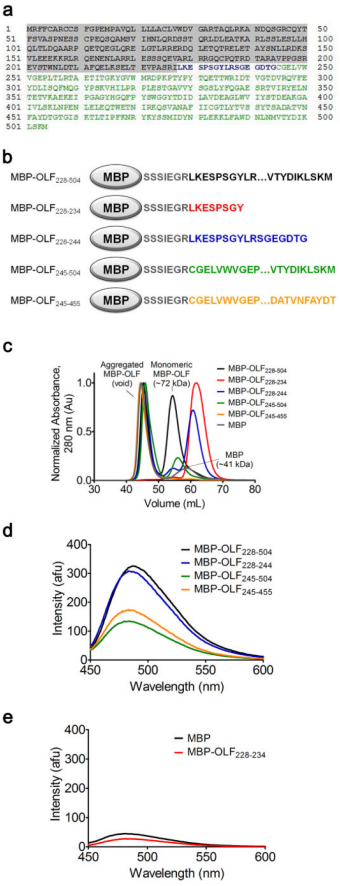

Figure 4.

Assembly of MBP-OLF fragments to identify regions of high amyloid propensity. (a) Myocilin sequence. Shaded area comprises the N-terminal signal sequence and coiled-coil not present in our OLF construct. Blue and green denote myoc-OLF. (b) Pictorial representation of MBO-OLF fragments discussed in text. (c) Overlay of Superdex 75 chromatograph of five MBP-OLF fragment constructs. (d) ThT fluorescence of void volume species isolated in (c). (e) ThT fluorescence of MBP and MBP-OLF$_{228-234}$ after incubation in a 37 °C water bath for 95 h with 0.5 mM SDS.

Table 1

Conditions that promote myoc-OLF fibrillization[a].

Additive	ThT Intensity, 485 nm (afu)
myoc-OLF (4 °C)	1.5 ± 0.9
0 mM SDS	0.8 ± 0.3
0.5 mM SDS	341.3 ± 35.6
0% H_2O_2	17.6 ± 5.3
1.5% H_2O_2	240 ± 6.4[b]
2.9% H_2O_2	27.3 ± 7.5

[a]All fluorescence intensity readings were acquired after 95 h incubation and are the average of two or more independent experiments.

[b]After 24 h incubation.